

INDEX

t refers to tables, f refers to figures.

Acetylene–metal copolymers, 43–44
“Active” polymer solution, 96
Ag–Au-alloyed clusters, 167
Ag–ClPPX films, 49, 51
Ag clusters, 48. *See also* Silver clusters
 stability of, 51
Ag–CNPPX films, 51
Agglomeration
 gold particle, 275–277
 silver particle, 278
Aggregate topology, 203–204, 205, 206
Ag–mercaptide powder, 169
Ag nanocrystals. *See also* Silver entries
 interaction of O₂ with, 11, 13f
 linear arrangements of, 16–17
 spectral characteristics and content of,
 50t
 two-dimensional arrays of, 18
Ag nanoparticles. *See* Silver
 nanoparticles
Ag particles, nonmagnetic circle, 232f.
 See also Silver particles
Ag–PMMA composites, 242
Ag–poly(chloro-*p*-xylylene) systems, 52
Ag–PPX, \bar{d} value for, 52
Ag–PPX systems, 48–49
Ag–PS nanocomposite film, 172–175
AgSC₁₂H₂₅–polystyrene blends, 176
Alcoholic reduction, 166
Alkanethiol, 168
Alkanethiolates, 180

Alkanethiol-derivatized gold clusters,
 158
 controlled synthesis of, 157
Alloy arrays, 19
Alloy nanocrystals, 4
Amorphous block copolymers, 43
Amorphous computing, 28
Anisotropic dark-field microscopy
 (ADFM), 227–228. *See also*
 Polarized anisotropic dark-field
 microscopy (ADFM)
Anisotropic nanocomposites, 265–282
Anomalous SAXS (ASAXS), 125. *See*
 also Small-angle X-ray scattering
 (SAXS)
Antiferromagnets, 210
Artificial atoms, ix
Assemblies, programmed, 15–24
Asymmetric Bruggeman formulas. *See*
 Hanai–Bruggeman formula
Atomic diffusion processes, 185
Au–Ag alloy nanocrystals, 4. *See also*
 Ag–Au- alloyed clusters
Au-based nanocomposites, synthesis of,
 156–158
Au nanocrystals, CO oxidation reaction
 and, 13–15. *See also* Gold entries
Au nanoparticles. *See* Gold nanoparticles
Au–polystyrene nanocomposite
 characterization, 158–166
Au–PVP nanocomposite system, 157

- Bands of regularity, 85, 87
 Belotelov, V. I., 201
 Bergman theory, 194
 Bimetallic nanoparticle synthesis, 137
 Bimodal crystal size distribution, 57
 Binding energy, 8
 Biphenylbutadiene groups, 176
 Bisarene complexes, cryochemically synthesized, 109
 Bloch lines, 227
 Block copolymer micelles
 cores of, 134–139
 coronas of, 139–142
 nanoparticles in, 134–144
 Block copolymers, 138
 Born approximation, 221
 Bottom-up processes, 76
 Bragg peak analysis, 125
 Bragg spacing, 147
 Bronstein, L. M., 123
 Bruggeman (BG) equation, 204, 206–207
 Bruggeman theory, 194
 “Cage” effect, 132
 Capping agents, 5
 Carbon-based composites, 257
 Carbon dioxide. *See* CO entries
 Carbon films, 79
 Carbon radicals, 178
 Carbonyl hydrides, 110
 Carbonyls, thermal decomposition of, 94–107
 Carbonyl thermolysis, peculiarities of, 101–102
 Carotenuto, G., 155
 Caseri, W., 265
 Catalytic activity
 size-dependent, 15
 of synthesized metal–polymer film materials, 67–70
 Catalytic isomerization, 67–68
 Cation–anion complexes, 105–106
 Cationic gel–anionic surfactant systems, 125–126
 C–Cl bond metathesis, 69–70
 catalytic reaction of, 68
 Centrosymmetric media, 216
 Cermet topology, 203–204, 205, 206
 CH₄ formation, 86–87
 Chain ion–radical clusterization, 95
 Chain process, 76
 Chain termination, 101
 Charge dynamic redistribution, 259
 Charge dynamic variation, 259
 Charge static redistribution, 257–258
 “Cherry-like” morphology, 135
 Chlorodecanes, 68
 Circular magnetic dichroism, 214. *See also* Magnetic circular dichroism
 “Cluspol” materials, 102
 Cluster aggregation, 38, 71
 Cluster beams, 3
 Cluster compounds, 4
 preparation of, 180
 Cluster formation, 111
 kinetics of, 115
 visualization of, 113, 114–116
 Cluster growth, mechanism of, 162
 Cluster-polystyrene solutions, 167
 Clusters
 stability of, 51
 temperature range and, 71
 CN–PX, 46
 CO (carbon monoxide) absorption, 13
 Cobalt. *See* Co entries;
 Octacarbonyl–dicobalt transformation scheme
 Co carbonyls, thermolysis of, 105
 Co compounds, 128
 Co-condensates, 38–39
 Co-deposition, 48
 CO formation, 86–87
 Coherent scattering region (CSR), 103
 Colloidal metal particle dispersions, fabricating, 96
 Colloids, polysilsesquioxane, 145–150
 Colorimetric sensing, 24–25
 Complexation, micelle formation via, 142–144

- Composite films, synthesized, 59
Composite media optics, 203–210. *See also* Magneto optics
Composites, conductivity of, 58
Computer modeling, of metallocopolymer nanocomposite assembly, 111–116
Co nanocrystals, arrays of, 18
Co nanoparticle formation, HPS and, 127–128
Co nanoparticles, 130–131
 sources of, 137
Conductivity
 humidity and, 60
 of synthesized metal–polymer film materials, 58–59
Confinement effects, ix
Controlled pyrolysis, of metal-containing precursors, 75–116
Controlled thermolysis, computer modeling of metallocopolymer nanocomposite assembly during, 111–116
Copper. *See* Cu²⁺–monoethanolamine complex; CuS–polyvinyl alcohol film
Copper-containing composite production, 109
Copper formate thermal decomposition, 108
Core-level binding energy, 8
Cotton–Mouton effect, 213
Coulombic states, 11
Cryochemical processes, 38
Cryochemical solid-state technique, 47
Cryochemical syntheses
 products of, 47
 solid-phase, 38–41
 vapor-deposition, 58, 70
Cryopolymerization, 48
Crystalline block copolymers, 4
Crystal size distribution, 573
Cu²⁺–monoethanolamine complex, 109.
 See also Copper entries
Curie group, 219
CuS–polyvinyl alcohol film, 61
Dark-field optical microscopy techniques, 226–228
Data processing systems, 63
Data recording, ultrahigh density, 202
Data storage, ferromagnetic nanoparticles and, 63–64
Dehydrolinalool (DHL), hydrogenation of, 137
Dekker Encyclopedia of Nanoscience and Nanotechnology, 124
Delphi program, 112
Demetallized polymer ligand, polymerization of, 111
Depolarization factors, 195, 197, 198, 208
Dichroic fibers, 268–269
Dichroic films, viii
 of poly(vinyl alcohol) and gold nanoparticles, 271–272
 poly(ethylene)–gold/silver nanoparticle, 272–281
Dichroic nanocomposites, 269, 282
 applications of, 279–280
Dichroic samples, preparation of, 267
Dichroism, 266
 extent of, 275
 origin of, 269–270
 in polymers containing metal nanoparticles, 266–270
Dielectric losses, 64, 65, 66
Dielectric matrices, embedding of nanoscopic metals into, vii
Dielectric properties, of synthesized metal–polymer film materials, 64–67
Dielectric relaxation, 65–66, 67
Differential scanning calorimetry (DSC), 164. *See also* DSC thermogram
Diffusion processes, 112
Diphenylbutadiene groups, 179
Dipole–dipole interactions, 173–175
Dip pen lithography, 24
d–l phase diagram, 20
Dodecanethiol (DDT), 157, 164
Draw ratios (DRs), 271–272, 275, 277–278

- Drying processes, 76
 DSC thermogram, 176. *See also*
 Differential scanning calorimetry
 (DSC)
 \bar{d} values, 51–52, 53, 54
 Dyadic Green function, 221
 Dzhardimalieva, G. I., 75
- Effective dielectric constant, formulas
 for, 204
 Effective dielectric functions, 194, 195,
 196
 Effective-medium approach, for
 magnetic composites, 209–210
 Effective-medium formulas, 205–207
 Effective-medium theory, 194, 198–199,
 203, 205
 “Effect of neighbor,” 81
 Electrical transport measurements, 25–
 27
 Electron beam irradiation, 186
 Electron diffraction analysis, 105
 Electronic structure, size-induced
 changes in, 9–10
 Electron microscopy, 186
 Elementary structural units (ESU), 205,
 206
 Ellipsoid particles, 207
 Maxwell Garnett theory for, 195–197
 Elliptical polarization, 214
 Embedded nanoparticles
 experimental, 185–188
 optical computations in exact route,
 188–194
 optical computations in statistical
 route, 194–198
 optical properties of, 184, 257
 plasmon absorption of, 183–199
 Embedded particles, size and shape
 variation in, 185
*Encyclopedia of Nanoscience and
 Nanotechnology*, 124
 Exact route, 184
 optical computations in, 188–194
 Exchange spring magnets, 27
- Ex-situ* Au-based nanocomposite
 synthesis, 156–158
 Extinction. *See* Optical extinction
 Extinction spectra, 191–193, 196,
 254–255, 256. *See also* Optical
 extinction spectra
- Faraday effect, 211, 212, 214
 Faraday rotation, 212
 Fe (iron) carbonyl complexes, 142–143
 Fe carbonyls, thermolysis of, 105.
 See also Fe(CO)₅
- Fe(CO)₅
 decomposition of, 102
 sonochemical decomposition of, 107
 thermolysis of, 96–99
- Fe-composites, x-ray diffraction
 characteristics of, 104t
- Fe–Pt alloy nanocrystals, 4
- Fermi level, 258
- Ferromagnetic materials, 229
- Ferromagnetic metals, plastics doped by,
 xi
- Ferromagnetic properties, of synthesized
 metal–polymer film materials,
 63–64
- Ferromagnetic resonance (FMR) spectra,
 Co particle, 128
- Ferromagnets, 210
- Ferrotricarbonyl complexes, 98
- Ferrum clusters, spatial periodicity of,
 103
- Filling factor, 207
- Film density, 64
- Film materials, synthesized
 metal–polymer, 57–70
- “Film on film,” 108
- FMR data, of HPS–Co samples, 128–129
- Fourier transforms, 222
- Gap states, 9
- Gas emission ability, 91–92
- Gas evolution, 81–82
 kinetics of, 89–90
 rates of, 83–85

- Gel–surfactant complexes, 125
Gel–surfactant ordering, 126
Geometry factors, 190–191
Gerasimov, G. N., 37
Giant clusters, 28–29
Giant nanocrystals, 22–24
Gold clusters, formation growth of, 161–162. *See also* Au entries
Gold colloids, 267–268
Gold–DDT clusters, 158
Gold-filled polystyrene films, 175
Gold nanoparticles
 in dichroic films, 271–281
 formation of, 135, 144
 in microgels, 144
 multilayers of, 22
 polymer-embedded, 158
 XRD pattern of, 159–161
Gold organosols, 18
Gold–polymer nanocomposite synthesis, 156–158
Granular materials, magneto optics of, 201–236
Green function Fourier transforms, 222
Green function technique, 209, 219–222, 231
Gyrotropic effects, 211
- Halide-containing matrices, metal carbonyl decomposition in, 103–104
Hamaker constant, 21
Hanai–Bruggeman (HBG) formulas, 204, 207–209
Havriliak–Negami empirical formula, 67
Heilmann, A., 183
Helmholtz equation, 220
High-dose ion implantation, 248
High-resolution transmission electron microscopy (HRTEM), x
Histograms, particle size distribution, 52–53
Homogenization technique, 205–207
Homoleptic mercaptides, 167–168
- HOMO–LUMO gap, 9, 10
Hydrogel–surfactant complexes, structural characteristics of, 127
Hydrogenation, 137
Hydrogen bond formation, 131
Hydrogen pressures, sensor response to, 62
Hydrophilic polymers, 166
Hypercrosslinked polystyrene (HPS), 127–134
 nanoscale cavities in, 130
- Imaging
 ADFM, 235–236
 high-resolution, 223
 magnetic dots, 229–236
 magneto optical, 202
 SNOM, 230–235
Inhomogeneous media, 220
In situ methods, 156
 metal–polymer nanocomposite synthesis, 167–168
Ion implantation, 241–260
Ion–insulator interaction, 249
Ionization energies (IE), 9
Ion synthesis, of metal nanoparticles, 247–252
Iron. *See* Fe entries; Ferrotetracarbonyl complexes
IR spectra, 89
- Kerr effect, 214–216
 magneto optical, 214–216
Kinetic processes, computer modeling and, 111–112
Kinetics, gas evolution, 89–90
Kohlrausch–Williams–Watts (KWW) expression, 66
Kubo gap, 7, 8
Kulkarni, G. U., 1
- Lamellar particles, HBG formula for, 208
Landau–Lifshitz equation, 229, 234
Large-angle X-ray powder diffraction (XRD), x

- Lead. *See* PbO entries; PbS entries
 Levi–Civita tensor, 211. *See also*
 Tensorial quantities
 Lichtenegger mixture equations,
 204–205
 Ligand-replacement reactions, 6–7
 Ligand shell tailoring, 5–7
 Linear inhomogeneous differential
 equations, 219
 Linear magnetic dichroism, 214
 Liquid crystal display (LCD), 279–282
 Longitudinal (meridional) Kerr effect,
 215–216
 Longitudinal MO effects, 216
 Long wavelength limit, 203
 Low-dose ion implantation, 248
 Low-temperature solid-state
 polymerization, 54, 71
- Magic nuclearity nanocrystals, 4–5
 arrays of, 18
- Magnesium. *See* Mg entries; PX–Mg
 co-condensation
- Magnetic circular birefringence, 211,
 212
- Magnetic circular dichroism, 212. *See also*
 Circular magnetic dichroism
- Magnetic composites, effective medium
 approach for, 209–210
- Magnetic data processing systems,
 high-density, 63
- Magnetic dots imaging, 229–236
- Magnetic elements, nanoscale, 229–236
- Magnetic force microscopy, 223
- Magnetic nanostructures, 202
- Magnetic objects, investigative methods
 for, 201–203
- Magnetic storage media, alternatives to,
 27
- Magnetization distributions, 223
- Magnetooptical (MO) imaging, 202.
 See also MO entries
- Magneto optics, 201–236
 composite media optics, 203–210
 Green functions approach, 219–222
- magnetic dots imaging, 229–236
 magnetooptical effects in transmission,
 211–214
 magnetooptical Kerr effect, 214–216
 nonlinear magnetooptical effects,
 216–219
 polarized anisotropic dark-field
 microscopy, 226–228
 scanning near-field optical
 microscopy, 223–226
 of uniform media, 210–211
- Manganese. *See* Mn–PX
 co-condensation
- Martorana, B., 155
- Maxwell equation, 220
- Maxwell Garnett (MG) formula, 204,
 206
- Maxwell Garnett theory, 194–196, 198
- Mercaptide–polystyrene systems, 168,
 172
- Mercaptides, 167–168
 thermolysis of, 175–176, 180
- Mesoscopic metals, viii–ix
- Metal acetylacetones, 79
- Metal acrylate thermal transformations,
 91–92
- Metal carbonyls
 decomposition trends in, 106
 polyionic ligands and, 103
 polymer-catalyzed decomposition of,
 100
 thermal decomposition of, 97–98
 thermolysis of, 95
- Metal carboxylated groups, stability of,
 87, 94
- Metal clusters, incorporated in polymer
 matrix, 47–57
- Metal-containing monomers, thermolysis
 of, 88–94
- Metal-containing polymer fragments,
 thermal decomposition of, 111
- Metal-containing polymer groups,
 decomposition of, 112
- Metal-containing polymers, 37–71
 decarboxylation of, 85

- solid-phase cryochemical synthesis of, 38–41
synthesis of, 38, 77
thermal decomposition of, 77–79
- Metal-containing precursors. *See also*
Metal-containing monomers;
Metal-containing polymers;
Metallocopolymer nanocomposites
controlled pyrolysis of, 75–116
metal sol formation, 94–107
post-thermolysis of, 107–110
transition metal polyacrylate
thermolysis, 79–88
- Metal fluoride formation, 105
- Metal hydroxide decomposition,
nanoparticle formation by, 108
- Metallated block copolymer micelles, 138
- Mettalation
of block copolymer micelle cores, 135
PAHAPS, 146–147, 149f
- Metallized polyione pyrolysis, 103
- Metallocopolymeric systems pyrolysis, 79
- Metallocopolymer nanocomposite
assembly, computer modeling of, 111–116
- Metallocopolymer nanocomposite
preparation, “bottom-up” and
“top-down,” 75–76
- Metallocopolymer nanocomposites,
synthesis of, 75–116
- Metallocopolymer production, by precursor
thermal decomposition, 102
- Metallocopolymer thermolysis, 79
solid-phase products of, 87–88
- Metal-nanocrystal-containing polymer
composite, 55
- Metal nanocrystals
density of states for, 7f
organization of, 17
- Metal nanoparticles (MNPs). *See also*
MNPs; Nanostructured polymeric
nanoreactors
dichroism in polymers containing, 266–270
embedding in a polymer matrix, 242
ion synthesis of, 247–252
optical extinction of, 241–260
optical properties of, 183
- Metal–nonmetal transition, 8
- Metal polyacrylates, thermolysis of, 79–88
- Metal–polymer complexes, structure of
cryochemically synthesized, 41–57
- Metal–polymer film materials
catalytic activity of, 67–70
conductivity and photoconductivity of, 58–59
dielectric properties of, 64–67
ferromagnetic properties of, 63–64
sensor properties of, 59–62
synthesized, 57–70
- Metal–polymer nanocomposite
formation, perspective method of, 88–89
- Metal–polymer nanocomposite synthesis, 155–180
Au–polystyrene nanocomposite
characterization, 158–166
gold–polymer nanocomposite
synthesis, 156–158
in situ, 167–168
metal precursor synthesis, 168–169
nanocomposite film characterization, 170–175
nanocomposite preparation, 166–167, 169
thermolysis mechanism, 175–179
- Metal–polymer nanocomposites
applications of, xi
design of, 123
history of, vii–viii
hydrogen reduction of, 130
optically anisotropic, 266–282
preparation of, ix
- Metal–PPX films, 58
- Metal precursor synthesis, 168–169
- Metals, nano-sized, xi–xii
- Metal sols, formation in polymers, 94–107

- Metal thiolates, 168
 Metal vapor synthesis techniques, 37–38
Mg–acrylonitrile co-condensate, 39. *See also* Organomagnesium structures
Mg clusters, 46
Mg–monomer complexes, 46
 Micelle cores, 134–139
 Micelle formation, via complexation, 142–144
 Micelles
 with embedded nanoparticles, 141
 hybrid, 141
 Micellization, of block copolymers, 142–144
 Microdiffraction patterns, 249
 Microgel crosslinking, 144
 Microgels, filled with Pd and Pt nanoparticles, 144–145
 Microscopy
 polarized anisotropic dark-field, 226–228
 scanning near-field optical, 223–226
 Mie electromagnetic theory, 247, 252–253, 260
 Mie resonance bands, 253
 Mixed carbonyls, 110
 MNPs. *See also* Metal nanoparticles (MNPs)
 formation of, 248–249
 synthesis of, 243–246
 Mn–PX co-condensation, 46–47
 MO dark-field microscopy, 227
 MOKE method, 229–230
 MO Kerr effects (MOKE), 214–216
 MO Kerr magnetometry, 202
 MO Kerr microscopy, 229
 Molybdenum. *See* MoS_x nanoparticles
 Monodisperse nanocrystal pellets, 25
 Monomers, thermal behavior of, 89
 Monophase metallopolymers, 103
 Monte Carlo method, 229
 MO SNOM development, 225
 MoS_x nanoparticles, 137–138
 Mott–Hubbard metal–insulator transition, 27
 Multiatomic particles, formation of, 112–113
 Multifunctional polysilsesquioxane colloids, nanoparticles in, 145–150
 Multilayer systems, 185
 Nanocavities, in polyoctadecylsiloxane, 131–133
 Nanoclusters, 1
 Nanocomposite films, 271
 characterization of, 170–175
 Nanocomposites
 Au-based, 156–158
 dichroic, 269
 formation of, 110, 111
 optical properties of, 265
 preparation of, 166–167, 169
 specific surface and topography of, 92
 ultrahigh/low refractive index optical, xi
 Nanocomposite synthesis, universal method for, 109
 Nanocomputing, 27–28
 Nanocrystal arrays, 16
 Nanocrystal assembly, 15–16
 Nanocrystalline film, Au, 3f
 Nanocrystals, 1–2
 applications for, 24–28
 chemical properties of, 11–15
 cluster aggregation to, 51
 electronic structure of, 7–9
 giant, 22–24
 incorporated in polymer matrix, 47–57
 ligand shell tailoring for, 5–7
 multilayer assemblies of, 21–22
 one-dimensional arrangements of, 16–17
 patterning of, 24
 physical properties of, 7–11
 programmed assemblies of, 15–24
 shape control of, 5
 size control of, 4–5
 surface area of, 11
 synthesis of, 2–4

- three-dimensional superlattice assemblies of, 21–22
two-dimensional arrays of, 18–21
- Nanoobjects. *See* Separate nanoobjects
- Nanoparticle morphology/shape control of, 156
modifying, 184–185
- Nanoparticles. *See also* Embedded nanoparticles; Metal nanoparticles in block copolymer micelles, 134–144 in multifunctional polysilsesquioxane colloids, 145–150 in polyelectrolyte microgels, 144–145
- Nanoparticle size, controlling, 123–124
- Nanoparticle synthesis, in the micelle corona, 139–142
- Nanoscale magnetic elements, 229–236
- Nano-sized metal particles, 155 applications for, 24–28
chemical properties of, 11–15
giant, 22–24
physical properties of, 7–11
programmed assemblies of, 15–24
properties of, 1–29
synthesis of, 2–7
three-dimensional superlattice assemblies of, 21–22
- Nanostructured materials, sonochemical synthesis of, 106–107
- Nanostructured metals, vii
- Nanostructured polymeric nanoreactors, 123–151 solid polymer nanostructures, 124–134 soluble polymer nanostructures, 134–150
- Nanotube formation, 103
- Negative magnetoresistance, 64
- Ni(Acr)₂ thermolysis, 93
- Nickel. *See* Ni(Acr)₂ thermolysis; Ni nanocrystals; PAA
- Nickel polyacrylate (NiPAc), 81 thermolysis of, 82–84, 85
- Nicolais, L., 155
- Ni nanocrystals, reaction of H₂S with, 11
- “Non-chain” inhibition method, 110
- Nonlinear Kerr effect, 217
- Nonlinear magnetooptical effects, 216–219
- Nonmagnetic circle Ag particle, 232f
- Nonmagnetic inhomogeneities, 232
- Nonspherical nanocrystals, 5
- Nonspherical particles, Maxwell Garnett theory for, 195
- Octacarbonyl–dicobalt transformation scheme, 99
- Octadecyltrichlorosilane, hydrolytic polycondensation of, 131
- ODMACl, 147–150
- Oligomers, liquid-like, 43
- One-dimensional nanocrystal arrangements, 16–17
- Optical computations in exact route, 188–194
in statistical route, 194–198
- Optical extinction, 241–260 experimental, 242–247 simulation of, 252–259
- Optical extinction spectra, 184, 187–188, 197–198. *See also* Extinction spectra
- Optically anisotropic metal–polymer nanocomposites, 265–282 dichroism in, 266–270 poly(ethylene)–gold/silver nanoparticle dichroic films, 272–281 poly(vinyl alcohol)–gold nanoparticle dichroic films, 271–272
- Optical magnetic anisotropy, 211
- Optical spectroscopy, x. *See also* UV–Vis spectroscopy “Optical theorem,” 205
- Optical wave, attenuation of, 252
- Optics. *See also* Magneto optics composite media, 203–210 of separate nanoobjects, 219–222
- Organomagnesium structures, synthesized, 44–47. *See also* Mg entries

- Organometallic compound
decomposition, nanoparticle formation by, 109–110
- Organometallic units, polymers containing, 42–47
- PAA, interaction of $\text{Ni}(\text{CH}_3\text{COO})_2$ with, 80
- PAHAPS-F1 colloids, 148
- PAHAPS-H4, 146f
- Palladium nanoparticles, 139. *See also* Pd entries
- Particle arrays
color of nanoparticles in, 266
formation of, 275
magnetization state of, 236
- Particle growth termination, 101
- Particle reshaping, 185–187
- Passivated metal particles, 156
- “Passive” polymer, 96
- Passive probe model, 225–226
- PbO–PPX films, 59, 60f, 61–62
- PbS concentration, increase in, 57
- PbS content, crystallite size distribution and, 55
- PbS–PPX films, 59
- PbS–PPX nanocomposite, 53
- Pd₅₆I nanocrystals, 23
- Pd colloids, 136, 140
- Pd nanocrystals
d–l phase diagram for, 20
I–V characteristics of, 12
- Pd nanoparticles
microgels filled with, 144–145
synthesis in HPS, 130
- Pd–PPX films, influence of hydrogen on, 62
- Pd–PPX nanocomposites, catalytic properties of, 68
- PdPt bimetallics, 137
- PdZn bimetallics, 137
- PEHP, 103, 110
- PEO-*b*-P2VP, 138–139
- PEO-*b*-PB, 138, 139
- PEO-*b*-PEI (polyethyleneimine), 143–144
- Percolation transition, 204
- Perlo, P., 155, 201
- PE–silver nanocomposites, 279
- PETF, 103–104, 105
- Phase behavior, of two-dimensional arrays, 20–21
- Phase inhomogeneities, 227
- Phase-object observation, 226f
- Phenyl rings, 130
- Photoconductivity, of synthesized metal–polymer film materials, 58–59
- Photocurrent response time, 59
- π -allylic complexes, polymer-immobilized, 98–99
- Plasma polymer thin films, 184
- Plasma resonance, 191
- Plasma resonance absorption, 188, 193–194
- Plasmon absorption, 183–199
- Plasmon bands, 9, 24
- Plasmon–polariton modes, 256
- Platinum. *See* Pt entries
- PODMACl–TANED colloids, 147–150
- PODS siloxy bilayers, nanoparticle formation in, 132–133
- Polar groups, particle growth and, 102
- Polarizability tensor, 189. *See also* Tensorial quantities
- Polarized anisotropic dark-field microscopy (ADFM), 226–228
- imaging in, 235–236
- Polar Kerr effect, 214–215
- Polar media, metal carbonyl decomposition in, 100
- Poly-AHAPS (PAHAPS) colloids, 146
- Polydentate ligand, 80
- Polydiallyldimethylammonium chloride (PDADMACl) gel, 125
- Polyelectrolyte gel–surfactant complexes, 124–134
- Polyelectrolyte microgels, nanoparticles in, 144–145
- Poly(ethylene)–gold/silver nanoparticle dichroic films, 272–281

- Polyethyleneimine (PEI), 116. *See also* PEO-*b*-PEI (polyethyleneimine)
- Polymer-based composite materials, designing, 241–242
- Polymer chains, thermal destruction of, 78
- Polymer composite materials, ferromagnetic nanoparticles in, 63–64
- Polymer-embedded metal nanostructures, novel properties in, x
- Polymer-embedded nanostructures, 155–156
- Polymer-embedding, vii, xii
- Polymeric films, xi
- Polymer-immobilized cobalt carbonyl, 104–105
- Polymer-immobilized nanoparticles, 103 production of, 107–108
- Polymerization, monomer, 39
- Polymerized system, nanoparticle growth in, 54
- Polymer matrices embedding metal nanoparticles in, 242 metal clusters and nanocrystals incorporated in, 47–57 post-thermolysis of precursors in, 107–110 thermal decomposition of metal carbonyls in, 97–98
- Polymer–metal particle interactions, 105
- Polymer nanoenvironment, designing, 151
- Polymer nanostructures solid, 124–134 soluble, 134–150
- Polymers. *See also* Metal-containing polymers containing organometallic units, 42–47 dichroism in, 266–270 formation of metal sols in, 94–107 thermolysis in the presence of, 96
- Polymer shell, 24
- Poly(methacrylic acid) cetylpyridinium chloride (PMA/CPC) gel, 125
- Polymethylmethacrylate (PMMA), 242, 243, 251–252, 253 silver implantation into, 254
- Polyoctadecylsiloxane, nanocavities in, 131–133
- PolyODMAC1 (PODMAC1) colloids, 147, 149–150
- Polyol process, 166
- Polysilsesquioxane colloids. *See* Multifunctional polysilsesquioxane colloids
- Polystyrene, hypercrosslinked, 127–134
- Polystyrene-*block*-poly-*m*-vinyltriphenylphosphine (PS-*b*-PPH), 143
- Polystyrene-embedded metal clusters, 170f
- Polystyrene films, 172 gold-filled, 175
- Poly(vinyl alcohol)–gold nanoparticle dichroic films, 271–272
- Pomogailo, A. D., 75
- Post-thermolysis, of metal-containing precursors, 107–110
- p-polarization, 231
- PPX composite films cryochemically synthesized, 59 negative magnetoresistance in, 64
- PPX–metal composites, catalytic properties of, 67
- PPX organomagnesium units, 44–47
- PPX–PbS composite, 55–56
- PPX supramolecular structure, 56
- Precursors, post-thermolysis of, 107–110. *See also* Metal-containing precursors
- Precursor thermal decomposition, 102
- Programmed assemblies, 15–24
- Prolate spheroids, optical extinction spectra for, 191
- PS-*b*-P4VP, 138
- Pt (platinum) nanocrystals, 16
- Pt nanoparticles, 141f microgels filled with, 144–145 synthesis in HPS, 130–131
- PVAL–gold nanocomposites, 271–272

- PVP-embedded gold clusters, 160, 166
 PVP/HAuCl₄ weight ratio, 159
 PX–Mg co-condensation, 44
p-xylene, 274–275
p-xylylene (PX) compounds,
 polymerization of, 39–40. *See also*
 CN–PX; Mn–PX co-condensation;
 PX–Mg co-condensation
p-xylylene monomers, 42
 Pyrolysis. *See* Controlled pyrolysis
- Quantum cellular automata, 28
 Quantum confinement, 2
 Quantum dots, 2
 Quantum-size effects, viii–ix
 Quantum states, size-dependent, 70
- Rao, C. N. R., 1
 “Raspberry-like” morphology, 135
 Rayleigh theory, 188–189, 198
 Rayleigh–Gans theory, 189, 194, 198
 RBS spectra, 249–251. *See also*
 Rutherford backscattering (RBS)
 Reflection SNOM, 224
 Research, nanocrystal, 2
 Reverse micellar methods, 2–3
 Rozenberg, A. S., 75
 Rutherford backscattering (RBS), 247.
See also RBS spectra
 R values, 69
- Salts, thermolysis of, 94
 Scalar free-space Green function, 220
 Scanning near-field optical microscopy
 (SNOM), 202, 223–226. *See also*
 SNOM configurations
 imaging in, 230–235
 Scanning tunneling spectroscopy (STS),
 9
 S–C bond cleavage reaction, 178
 Second harmonic generation effect, 216,
 217
 Second-order surface polarization,
 217–218
 Self-aggregation process, 22–24
- Semiconductor nanocrystals, 4
 Separate nanoobjects, optics of, 219–222
 SET (single-electron transistor) arrays,
 27–28
 Shape factor, 187
 Silver clusters, 173. *See also* Ag clusters
 Silver core–carbon sheath interface,
 effects at, 257–259
 Silver dodecyl mercaptide, 168–169
 Silver ion implantation, 249–252
 Silver nanoparticles. *See also* Ag entries
 in dichroic films, 272–281
 embedded, 192f
 extinction of, 254–255
 extinction spectra for, 253
 Silver particles. *See also* Ag particles
 extinction of, 252–256
 extinction with carbon shell, 256–257
 Silver–polystyrene nanocomposite films,
 preparing, 169
 Silver trifluoroacetyl–acetone, thermal
 decomposition of, 108
 Small-angle X-ray scattering (SAXS),
 56, 125
 SNOM configurations, 224f
 SNOM microscopy, 230–235. *See also*
 Scanning near- field optical
 microscopy (SNOM); Transmission
 SNOM
 Sol–gel reaction, 145, 147
 Solid-phase cryochemical synthesis,
 38–41
 Solid-phase diffusion, 112
 Solid-phase products, topography and
 composition of, 93
 Solid polymer nanostructures, 124–134
 Solid state, thermal decomposition in, 76
 Solid-state polymerization,
 low-temperature, 71
 Solid-state synthesis, 70
 Solid-vapor-deposited metal–monomer
 co-condensates, 39
 Soluble polymer nanostructures,
 134–150
 Sonoluminescence, 106

- Spectral density function, 194
Spectroscopy, dielectric, 64
Spheric aggregates, 279
Spherical/spheroid particles, 190–191
 HBG formula for, 207–208
 particle size of, 187
s-polarization, 231
SPR absorption, 252. *See also* Surface plasma resonance (SPR)
SPR absorption spectra, 258
SPR band intensity, 257
SPR extinction band, 258
Statistical route, optical computations in, 194–198
Stepanov, A. L., 241
Styrene radical polymerization, 179
Superlattices, three-dimensional, 21–22
Surface atoms, 70
Surface-deposition, controlled kinetic, 164
Surface effects, ix
Surface-modified particles, 273–274
Surface nonlinear optical polarization, 217–218
Surface passivation, 156
Surface plasma resonance (SPR), 241.
 See also SPR entries
Surface plasmon
 absorption of, 172
 excitation of, 183
Surface plasmon resonance, x, xi, 206
Surfaces, patterns of nanocrystals on, 24
Surface tunneling microscopy (STM), vii
Surfactant counterions, 141
Surfactant head groups, 141–142
Surfactant molecules, 124
Synthesis methods, 28
Synthesized metal–polymer film materials
 catalytic activity of, 67–70
 conductivity and photoconductivity of, 58–59
 dielectric properties of, 64–67
 ferromagnetic properties of, 63–64
 physicochemical properties of, 57–70
 sensor properties of, 59–62
Synthetic strategies, 2–7
TANED, 147–150
Tensorial quantities, 209–210. *See also* Levi–Civita tensor; Polarizability tensor
Teramac computer, 28
Thermal decomposition, 75
 carbonyl, 94–107
 of metal-containing polymers, 77–79
 solid-phase products of, 86
Thermally induced particle reshaping, 187
Thermal methods, 116
Thermal transformations, kinetic studies of, 89
Thermochromic effect, 169, 172–173
Thermogravimetric analysis (TGA), 164
Thermolysis, 75, 175–179
 gaseous product yield from, 86
 macromolecular structure during, 85
 of metal-containing monomers, 88–94
 of transition metal polyacrylates, 79–88
Thioaurite compounds, synthesis of, 157
Thiolates, 168
Thiol-derivatized gold clusters, 166–167, 179
Thiol-derivatizing hydrosols, 6–7
Thiolized metal nanocrystals, 18
Thiolized Pd nanocrystals, hexagonal arrays of, 19
Thomas, P. J., 1
Three-dimensional superlattices, 21–22
Time-temperature superposition principle, 67
Topology. *See* Aggregate topology; Cermet topology
Trakhtenberg, L. I., 37
Transformation scheme, 111

- Transition metal polyacrylates,
thermolysis of, 79–88
- Transition metals, mercaptides of,
167–168
- Transmission, magnetooptical effects in,
211–214
- Transmission electron microscopy
(TEM), x, 158, 170, 184
- Transmission SNOM, 223–224. *See also*
Scanning near-field optical
microscopy (SNOM)
- Triethylene-diaminic complex,
thermolysis of, 108
- Tunnel electron transfer processes, 58
- Two-dimensional arrays, 18–21
conductivity of, 27
stability and phase behavior of,
20–21
- Uniform media, magneto optics of,
210–211
- UV–Vis spectra, 44, 45f, 272, 277, 279
of solid films, 49f, 50f
- UV–Vis spectroscopy, 161–162, 163
- van der Waals interaction, 21
- Vapor-deposition solid-state synthesis,
57–58
- Vapor synthesis methods, 37–38
- Vertical Bloch lines (VBLs), 227, 228f
- Voigt effect, 213–214
- Volume filling factor, 194, 196
- Water–toluene interface, nanocrystal
synthesis at, 3
- Wetting processes, 76
- Xe-ion implantation, 247
- X-ray diffraction data, 93
- Zinc. *See* PdZn bimetallics
- Zvezdin, A. K., 201



Figure 9.1. Microscope image of a dichroic nanocomposite consisting of gold particles embedded in wood (probably fir), published in 1905 [36]. The polarization plane of the light is parallel to the orientation axis of the wood in the left image and perpendicular in the right image.

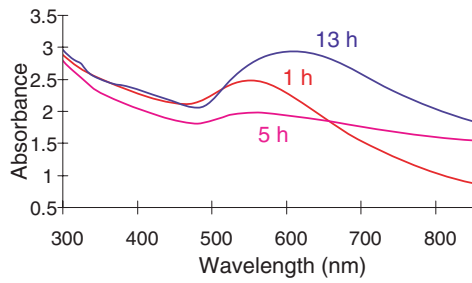
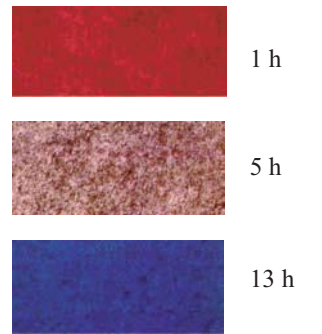


Figure 9.7. Colors and UV-Vis spectra of dispersions of gold particles (average diameter 2.2 nm, covered with a layer of 1-dodecanethiol) kept in a poly(ethylene) solution in *p*-xylene at 130°C for 1 hr, 5 hr, and 13 hr, respectively.

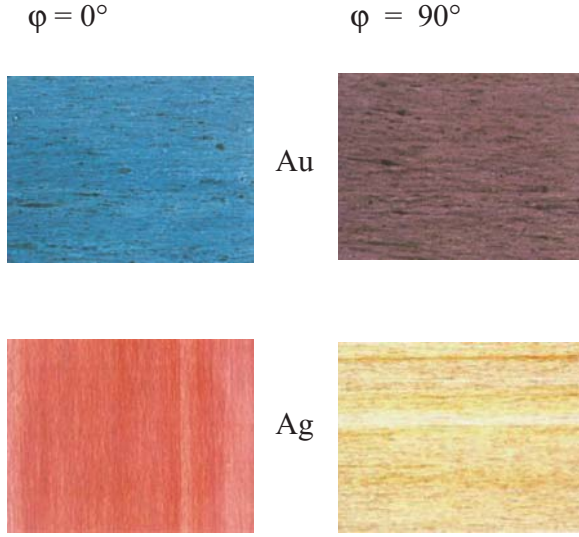
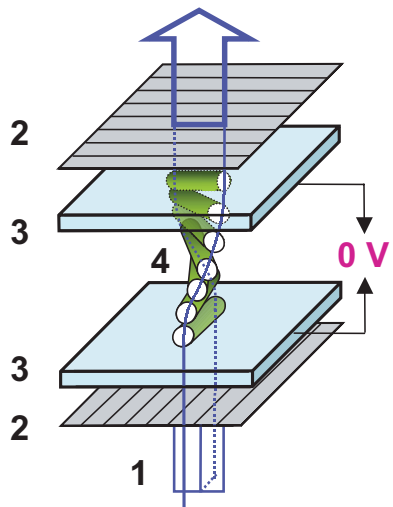
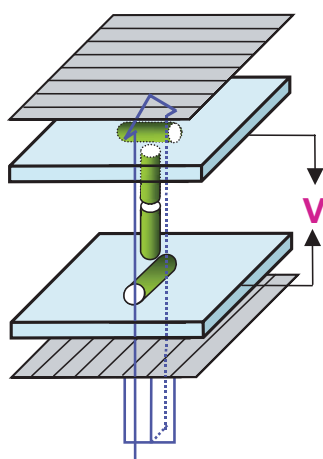


Figure 9.9. Colors of a drawn poly(ethylene)-gold and a poly(ethylene)-silver nanocomposite in polarized light with the polarization plane of the incident light and the drawing direction of the nanocomposite parallel ($\phi = 0^\circ$) and perpendicular ($\phi = 90^\circ$), respectively.

transmission of light

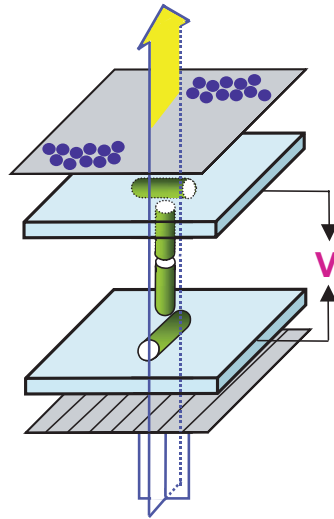
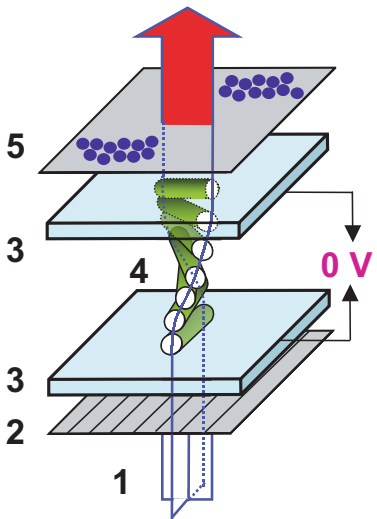


complete light absorption



(a)

light transmission in both states but in different colors



(b)

Figure 9.12. Schematic representation of (a) a standard twisted-nematic liquid crystal display and (b) a related display equipped with a drawn nanocomposite. 1, incoming light (unpolarized); 2, polarizer; 3, glass plate coated with an electrode layer and an orientation layer for the liquid-crystalline molecules; 4, liquid-crystalline molecules forming a 90° helical twist in absence of a voltage or a linear array parallel to an electric field in presence of an electric field; 5, nanocomposite with oriented arrays of metal particles.

COLOR PLATES



Figure 9.13. A twisted-nematic liquid crystal display (LCD) equipped with a poly(ethylene)-silver nanocomposite that had been annealed at 180°C for 15 hr and subsequently drawn as described in the text. The drawing axis of the nanocomposite is oriented parallel to the polarizer in the left image and perpendicular in the right image.